# Mitigation of the double ITCZ syndrome in BCC-CSM2-MR through improving parameterizations of boundary-layer turbulence and shallow convection

Yixiong Lu[1], Tongwen Wu[1], Yubin Li[2], Ben Yang[3,4]

5    [1]Beijing Climate Center, China Meteorological Administration, Beijing, 100081, China
[2]School of Atmospheric Physics, Nanjing University of Information Science and Technology, Nanjing, 210044, China
[3]School of Atmospheric Sciences, Nanjing University, Nanjing, 210023, China
[4]CMA-NJU Joint Laboratory for Climate Prediction Studies, Nanjing University, Nanjing, 210023, China

10    *Correspondence to*: Yixiong Lu (luyx@cma.gov.cn)

**Abstract.** The spurious double intertropical convergence zone (ITCZ) is one of the most prominent systematic biases in coupled atmosphere-ocean general circulation models (CGCMs), and the underestimated marine stratus over eastern subtropical oceans has been recognized as a possible contributor. Rather than modifying the cloud scheme itself, this study significantly promotes the marine stratus simulation through improving parameterizations of boundary-layer turbulence and

15    shallow convection in the medium-resolution Beijing Climate Center Climate System Model version 2 (BCC-CSM2-MR). The University of Washington moist turbulence scheme is implemented in BCC-CSM2-MR to better represent the stratocumulus, and a decoupling criterion is also introduced to the shallow convection scheme for improving the simulation of the stratocumulus-to-cumulus transition. Results show that the simulated precipitation in the eastern Pacific south of the equator is largely reduced, alleviating the double ITCZ problem. The tropical precipitation asymmetry index increases from

20    −0.024 in the original BCC-CSM2-MR to 0.147 in the revised BCC-CSM2-MR, which is much closer to the observation. The study suggests that improving parameterizations of boundary-layer turbulence and shallow convection is effective for mitigating the double ITCZ syndrome in CGCMs.

## 1 Introduction

The coupled atmosphere-ocean general circulation models (CGCMs) have been widely used in the studies of climate

25    variability, change and prediction. Despite decades of development, there are still many systematic biases in CGCMs, hampering the reliability of model results and limiting their utility. A prominent tropical bias in generations of CGCMs is the double intertropical convergence zone (ITCZ) syndrome, which is characterized by two parallel zonal bands of annual precipitation straddling the equator over the central and eastern Pacific, while it is absent in the observations (Mechoso et al., 1995; Lin, 2007; Zuidema et al., 2016; Zhang et al., 2019). The observed convergence zone south of the equator extends

30    southeastward from the western Pacific, whereas most CGCMs simulate a southern zonal rainfall band extending too far

eastward. This bias is often associated with excessive warm sea surface temperatures (SSTs) in the southeastern Pacific (SEP). Similarly, in the tropical Atlantic basin, most CGCMs present a fake southern zonal convergence zone, mirroring the actual zonal convergence zone north of the equator. The spurious double ITCZ not only affects the intensity of the Hadley circulation and the distribution of the trade winds directly related to the simulation of El Niño events, but also creates biases

35 of latent heating in the tropics that can impact midlatitude weather and climate through atmospheric teleconnections (Schneider et al., 2009; Manganello and Huang, 2009).

The double ITCZ syndrome in CGCMs has been a long-standing problem, and it remains a serious impediment. In earlier phases of Coupled Model Intercomparison Project (CMIP), from Phase 3 (CMIP3) to Phase 5 (CMIP5), most CGCMs suffered from the double ITCZ problem to various degrees (Lin, 2007). Compared with CMIP3 models, there is no

40 evidence of improvements in reducing the excessive precipitation and warmer SST in the SEP by the CMIP5 models, with results from CMIP5 somewhat worse than those from CMIP3 (Zhang et al., 2015). In the latest CMIP6, the biases persist in some of the current state-of-the-art CGCMs (Williams et al., 2018; Wu et al., 2019), indicating that it remains a tough challenge to alleviate the double ITCZ bias in CGCMs.

Many efforts have been devoted to identifying the possible contributors to the double ITCZ problem, and both oceanic

45 and atmospheric causes are suggested (Zhang et al., 2019). For instance, by restoring model ocean temperature and salinity to observations in the upper ocean, the effects of ocean eastern boundary biases along the Peruvian-Chilean coast was investigated, and it was found that the coastal SST and salinity biases exert significant influences on the SEP precipitation (Large and Danabasoglu, 2006). Modelling studies show that the double ITCZ bias is very sensitive to atmospheric processes, such as convections and cloud. As ITCZ precipitation originates from convections, convection parameterization

50 schemes are often blamed for the double ITCZ problem. By modifications in closure, trigger function, and lateral entrainment of the convection scheme, the double ITCZ can be mitigated to varying degrees (Song and Zhang, 2009; Zhang and Song, 2010; Queslati and Bellon, 2013; Song and Zhang, 2018). Deficiencies in the extratropical cloud simulation are also suggested to be possible causes of the tropical double ITCZ (Hwang and Frierson, 2013; Li and Xie, 2014). It is argued that the negative cloud amount biases over the Southern Ocean and the associated warming can induce anomalous northward

55 cross-equatorial atmospheric energy transport, resulting in a meridional shift of ITCZ. However, based on this atmospheric teleconnection argument and by reducing the shortwave radiation bias over the Southern Ocean in the fully coupled National Center for Atmospheric Research (NCAR) Community Earth System Model version 1 (CESM1), Kay et al. (2016) found that the double ITCZ is not improved.

The negative cloud amount biases off the west coast of South America, which are common in CGCMs, are regarded as

60 another cause for the double ITCZ problem. It is believed that the underestimated cloud cover leads to more net heat flux into the ocean and the warm SST biases in the SEP, which is associated with stronger convections and precipitation. Previous studies to ameliorate the double ITCZ bias mostly focused on the role of the cloud fraction parameterization, either through prescribed increases or through physical parameterization changes (Ma et al., 1996; Yu and Mechoso, 1999; Dai et al., 2003, 2005; Qin and Lin, 2018). Furthermore, increased cloud fraction and the associated shortwave cloud forcing over

65 the SEP can be driven by changes in representation for cloud microphysics (Woelfle et al., 2019). Modifications on the cloud scheme itself are helpful to mitigate the double ITCZ to some extent; however, it still plagues most CGCMs.

Rather than directly modifying the cloud macro/microphysics schemes in CGCMs, this study changes parameterizations of the boundary-layer turbulence and shallow convection to improve the low-level cloud simulation indirectly. The low-level cloud near the South American west coast is the steadiest and most persistent stratocumulus regime in the world, which is

70 closely related to multiple processes, such as boundary layer (BL) mixing, surface sensible and latent heat fluxes, cloud-top radiative cooling, and entrainment (Wood 2012). Furthermore, a prominent feature of the low-level cloud in the SEP is that the stratocumulus regime progressively transforms into the trade cumulus regime moving downstream off the coast. In the transition, interactions between BL turbulence and shallow convection play a critical role. When multiple separate BL and shallow convection schemes are combined to complement each other in a CGCM, inconsistencies between parameterizations

75 are likely to be introduced. This study aims to find out whether improving parameterizations of BL turbulence and shallow convection accounts for the double ITCZ bias in CGCMs. This is done through a two-step process, using the medium resolution Beijing Climate Center Climate System Model version 2 (BCC-CSM2-MR). The first step is to determine if the stratocumulus simulation is improved with prescribed SSTs through modifying parameterizations of BL turbulence and shallow convection in the atmospheric component of BCC-CSM2-MR. The second step, which indicates the atmosphere-

80 ocean feedback, is to perform a pair of ocean-atmosphere coupled simulations to demonstrate the impact of improved stratocumulus representation on the simulation of the SSTs and precipitation in the SEP.

The paper is organized as follows. Section 2 describes the BCC-CSM2-MR, focusing on the new configurations of the BL and shallow convection schemes, as well as the model setups for the control and sensitive experiments. A brief review of the observational data used to evaluate the model results is also included. Section 3 compares the cloud simulation results

85 from the atmosphere-only runs, and section 4 discusses the impact of improved cloud simulation on the SSTs and precipitation in the coupled runs. Further discussion on the effectiveness of the new configuration of the BL turbulence and shallow convection parameterizations is shown in section 5. At last, section 6 presents the summary and conclusions.

## 2 Model description, experimental design, and observational data

### 2.1 Brief description of the BCC-CSM2-MR

90 In the present study, we use the version of BCC-CSM2-MR participating in CMIP6, which is a fully coupled model with atmosphere, ocean, land surface, and sea ice components (Wu et al., 2019). The atmospheric component in BCC-CSM2-MR is based on the Beijing Climate Center atmospheric general circulation model (BCC-AGCM; Wu et al., 2010). The spectral dynamical core of BCC-AGCM is featured by introducing a reference stratified atmospheric temperature and a reference surface pressure into the governing equations (Wu et al., 2008). The Beijing Climate Center Atmosphere-Vegetation

95 Interaction Model (BCC-AVIM; Li et al., 2019) serves as the land component of BCC-CSM2-MR. It includes major land surface biophysical and plant physiological processes. The oceanic component is based on the Modular Ocean Model

version 4 (MOM4; Griffies et al., 2005) and the sea ice component is the Sea Ice Simulator (SIS; Winton, 2000). Over the sea ice, a new bulk aerodynamic algorithm is formulated for computing surface exchange fluxes (Lu et al., 2013). The above four components are physically coupled through fluxes of momentum, energy, and water at their interfaces, which is realized

100    using the NCAR flux coupler version 5.

The atmospheric component of BCC-CSM2-MR has a horizontal resolution of T106 (approximately 1.125° latitude by 1.125° longitude) with 46 hybrid vertical levels. The deep convection scheme used in BCC-CSM2-MR is based on a mass-flux bulk cloud model approach, in which the mass change for the adiabatic ascent cloud parcel with altitude is derived from a total energy conservation equation of the whole adiabatic system involving the updraft cloud parcel and the environment

105    (Wu 2012). Compared with its previous version in CMIP5, BCC-CSM2-MR has notably improved the simulation skills of atmospheric variability in the tropics, such as the Madden-Julian oscillation and the stratospheric quasi-biennial oscillation (Wu et al., 2019; Lu et al., 2020).

However, the version of BCC-CSM2-MR participating in CMIP6 still suffers from the double ITCZ syndrome. The mean precipitation errors are dominated by systematic errors along the ITCZ. Here we show that a revised version of BCC-

110    CSM2-MR, configured with new parameterizations of BL turbulence and shallow convection, significantly reduces the double ITCZ bias.

### 2.2 Parameterization of BL processes

The CMIP6 configuration of the BCC-CSM2-MR employs the Holtslag and Boville (1993) parameterization (hereafter called the HB scheme), which is optimized for the simulation of dry convective BLs over land. The HB scheme is based on

115    the eddy diffusivity approach. And the eddy diffusivity of variables $\chi$ is given by

$$K_\chi = k w_\chi z \left(1 - \frac{z}{h}\right)^2 , \tag{1}$$

where $k$ is the von Karman constant; $z$ is the height; $w_\chi$ is a turbulent velocity; and $h$ is the boundary layer height. For neutral and stable conditions, $w_\chi$ is proportional to the friction velocity, while for unstable conditions, $w_\chi$ is proportional to the convective velocity scale $w_*$

120

$$w_* = \left[\frac{g}{\theta_{vs}} h \overline{\left(w'\theta_v'\right)_s}\right]. \tag{2}$$

Here, $g$ is the gravitational acceleration; $\theta_{vs}$ is the virtual potential temperature at surface; and $\overline{\left(w'\theta_v'\right)_s}$ represents the buoyancy heat flux at surface. The above formula suggests that the HB scheme assumes the BL turbulence to be forced exclusively from the surface heating and friction velocity.

In the marine stratocumulus-capped BLs, the turbulence structure depends strongly on the dominant turbulence

125    generating mechanism resulting from both evaporative and radiative cooling at cloud top. To provide a more physically

realistic treatment of stratocumulus-topped BLs, the University of Washington moist turbulence (UWMT) scheme from Bretherton and Park (2009) is implemented in the revised BCC-CSM2-MR to replace the HB scheme. The UWMT scheme also uses first-order $K$ diffusion to represent all the turbulence, in which the eddy diffusivity is calculated based on the turbulent kinetic energy (TKE, $e$) and proportional to the stability-corrected length scale $lS_\chi$, given by

130
$$K_\chi = lS_\chi \sqrt{e} . \tag{3}$$

In the case of an inversion layer at the top of convective BLs, the diffusivities are parameterized as following

$$K_\chi = w_e \Delta z_e , \tag{4}$$

where $w_e$ is the entrainment rate, and $\Delta z_e$ is the thickness of the entrainment layer. The UWMT scheme uses the $w_*$ entrainment closure raised by Nicholls and Turton (1986):

135
$$w_e = A \frac{w_*^3}{\left(g \Delta^E s_{vl} / s_{vl}\right)\left(z_t - z_b\right)} . \tag{5}$$

Here, $z_t$ and $z_b$ are the top and bottom heights of the entrainment layer, respectively; $\Delta^E$ denotes a jump across the entrainment layer; and $s_{vl}$ is the liquid virtual static energy. $A$ is a nondimensional entrainment efficiency, which is affected by evaporative cooling of mixtures of cloud-top and above-inversion air.

### 2.3 Shallow cumulus Parameterization

140     To treat shallow cumulus, the original version of the BCC-CSM2-MR adopts a stability-dependent mass-flux representation of moist convective processes with the use of a simple bulk three-level cloud model, as in Hack (1994). Specifically, in a vertically discrete model atmosphere where the level index $k$ decreases upward and layers $k$ and $k+1$ are moist adiabatically unstable, the Hack scheme assumes that there is a non-entraining convective element with roots in level $k+1$, condensation and rain out processes in level $k$, and limited detrainment in level $k-1$. By repeated application of this procedure from the bottom of the model to the top, the thermodynamic structure is locally stabilized.

145         The Hack shallow cumulus scheme can be also active in moist turbulent mixing, such as stratocumulus entrainment, which has different physical characteristics than cumulus convection. Shallow cumulus is usually regarded as a decoupled BL regime, in which the vertical mixing processes do not achieve a single well-mixed layer, while the stratocumulus regime represents a well-mixed BL up to the cloud top. The decoupling criterion to distinguish the two regimes is of great

150 importance for simulating the stratocumulus-to-cumulus transition (Bretherton and Wyant, 1997; Wood and Bretherton, 2004). A number of these decoupling criteria have been explored, such as static stability (Klein and Hartmann, 1993) and the buoyancy flux integral ratio (Turton and Nicholls, 1987). In the light of its robustness, the stability criterion with a threshold of 15 K is introduced into the Hack scheme. The lower tropospheric stability (*LTS*) is defined as

$$LTS = \theta_{700hPa} - \theta_{sfc} \ , \tag{6}$$

155 where $\theta_{700hPa}$ and $\theta_{sfc}$ are potential temperatures at 700 hPa and surface, respectively. In the revised BCC-CSM2-MR, the Hack scheme is activated only in the decoupled BL regimes with $LTS < 15$ K below 700 hPa. Above 700 hPa, the Hack scheme is retained to remove any local instability as long as the two adjacent model layers are moist adiabatically unstable.

### 2.4 Cloud fraction parameterization

160 In the original BCC-CSM2-MR, the cloud amount is evaluated via a diagnostic method, depending on relative humidity, convective mass fluxes and atmospheric stability (Wu et al., 2019). Three types of clouds are diagnosed: layered stratus cloud, convective cloud, and low-level marine stratocumulus. The marine stratocumulus cloud fraction is particularly parameterized to compensate the HB dry turbulence scheme. It is calculated by using an empirical relationship between the observed stratocumulus cloud amount and the boundary layer stratification, which is evaluated with potential temperatures at 165 700 hPa and surface, as in Klein and Hartmann (1993).

Considering the advantage of the UWMT scheme to simulate marine stratocumulus, the revised BCC-CSM2-MR excludes the empirical calculation of stratocumulus cloud amount and only uses the relative humidity and convective cloud fraction to deduce the overall cloud amount. The stratocumulus cloud fraction is assumed to be diagnosed from relative humidities. The critical relative humidities $RH_c$ are used to tune the global annual mean top-of-atmosphere (TOA) shortwave 170 and longwave radiative energy fluxes close to observations. The original BCC-CSM2-MR uses the low-level (below 750 hPa) $RH_c$ of 0.945, while the revised BCC-CSM2-MR uses the low-level $RH_c$ of 0.97. Given the exclusion of special stratocumulus cloud fraction parameterization and increment in the low-level $RH_c$ in the revised BCC-CSM2-MR, better simulation skills of low-level cloud are attributed to the improved schemes of BL turbulence and shallow convection.

### 2.5 Experimental design

175 Table 1 summarizes all the experimental setups. Two sets of 11-yr Atmospheric Model Intercomparison Project (AMIP)-type simulations are conducted with the same prescribed sea surface boundary conditions using the Hadley Centre SSTs and sea ice concentrations. The one using the default configurations of HB and Hack schemes is referred to as REF_amip, and the other using the new configurations of UWMT and modified Hack schemes is referred to as NEW_amip. For each integration, the first year is treated as the spinup, and the last 10 years are used for analysis. Both runs start from identical 180 initial conditions. Note that the Cloud Feedback Model Intercomparison Project Observation Simulator Package (COSP; Bodas-Salcedo et al., 2011) is turned on to better compare with satellite observations.

For the fully coupled experiments, two sets of 12-yr Coupled Model Intercomparison Project (CMIP)-type simulations are carried out under pre-industry conditions, using greenhouse gases, ozone, aerosol emission, and others fixed at the level

of 1850. The CMIP simulation with the default HB and Hack schemes is referred to as REF_cmip, whereas the simulation

185    using the UWMT and modified Hack schemes is referred to as NEW_cmip. Both runs are initialized with the data sets at the
345th year of a pre-industry control run provided by the default BCC-CSM2-MR. Theses initialization data sets are close to
the equilibrium state. Note that previous studies have shown that the formation and mitigation of the double ITCZ biases can
be completed within the first 2 years of simulation (Liu et al., 2012). Therefore, a 12-yr integration for each coupled
experimental setup is performed, of which the first 2 years are treated as the spinup, and the last 10 years are used for

190    analysis.

To highlight the relative roles of the UWMT scheme and the modified Hack scheme in the low-level cloud simulation
in NEW_amip, two extra AMIP-type sensitivity experiments are designed. The modifications of the boundary-layer
turbulence scheme and the shallow convection scheme are added, respectively in the two sensitivity experiments. The
simulation with changes only in the boundary-layer turbulence scheme is referred to as UWMT_amip, whereas the

195    simulation with changes only in the shallow convection scheme is referred to as mHack_amip. The difference between
UWMT_amip and REF_amip will show the isolate impact of change in the boundary-layer turbulence parameterization,
while the difference between mHack_amip and REF_amip will show the isolate impact of change in the shallow convection
parameterization.

### 2.6 Observational data

200    To evaluate the simulated cloud amount and shortwave cloud radiative forcing (SWCRF), the distribution of cloud fraction
from the CALIPSO GOCCP data set (GCM-Oriented CALIPSO Cloud Product; Chepfer et al., 2010) and TOA SWCRF
from the CERES-EBAF data set (Clouds and the Earth's Radiant Energy System Energy Balanced and Filled data product;
Loeb et al., 2018) are used as references. The simulated precipitation is compared with the Global Precipitation Climatology
Project (GPCP) monthly precipitation analysis (Adler et al., 2003) for years 1981 to 2010. Considering the uncertainty in

205    precipitation observations, the Climate Prediction Center (CPC) Merged Analysis of Precipitation (CMAP; Xie and Arkin,
1997) from 1981 to 2010 is also used. Additional observations include SSTs from the Hadley Centre Sea Ice and Sea Surface
Temperature data set (HadISST; Rayner, 2003), and wind velocities from the Japanese Meteorological Agency 55-year
Reanalysis (JRA-55; Kobayashi et al., 2015).

### 3 Improved cloud representation in the atmosphere-only simulations

210    ### 3.1 TOA SWCRF

TOA SWCRF is one of the most important metrics to examine for improving the representation of low-level clouds. Figure 1
compares annual mean TOA SWCRF simulated by REF_amip with CERES-EBAF observations. The global mean SWCRF
is −45.83 W m$^{-2}$ in CERES-EBAF and −49.51 W m$^{-2}$ in REF_amip. REF_amip simulates the SWCRF distributions relatively
well, but overestimates the magnitude of SWCRF over regions of Northern Hemisphere storm tracks and underestimates the

215   magnitude of SWCRF over the subtropical marine stratocumulus regions. Compared with REF_amip (Figure 1d), NEW_amip shows a considerably increased simulated magnitude of SWCRF over the eastern subtropical ocean regions, suggesting that the low-level cloud representation is improved with new configurations of BL turbulence and shallow convection schemes.

### 3.2 Low-level cloud cover

220   TOA SWCRF strongly depends on the low-level cloud fraction. As shown in Figure 2a, the observed low cloud is prevalent over midlatitude storm-track regions, eastern tropical and subtropical oceans and the Southern Ocean. Figure 2b and 2c present the simulated annual mean low-level cloud amount from REF_amip and NEW_amip, respectively. Generally, both simulations reproduce the observed patterns of low-cloud amount with maxima in the midlatitude storm tracks and minima in the trade cumulus regime over the ocean. One prominent discrepancy between REF_amip and observations is a

225   remarkable underestimation of low-cloud fraction over the eastern subtropical oceans, which contributes to the weak bias in the magnitude of TOA SWCRF over these regions in REF_amip. The observed maxima in the subtropical stratocumulus decks are better simulated by NEW_amip. The global mean low-level cloud fraction increases from 24.64% in REF_amip to 28.74% in NEW_amip, closer to 37.06% in the GOCCP observations. With new configurations of BL turbulence and shallow convection parameterizations, the low-cloud fraction is significantly increased by up to 40% over the eastern

230   subtropical oceans (Figure 2d).

### 3.3 The subtropical Stratocumulus-to-Cumulus (Sc-to-Cu) transition

In order to further illustrate the consistency between the UWMT turbulence scheme and modified Hack shallow convection scheme, Figure 3 shows vertical cross sections of cloud fraction depicting the subtropical stratocumulus to trade cumulus transition both in the observations and simulations. We focus on the five main regions of the subtropical Sc-to-Cu transition,

235   with the locations shown in Figure 2a. Observational guidance is provided from GOCCP. GOCCP generally shows a clear transition from stratocumulus near the coast to trade cumulus well offshore, marked by a gradual reduction of cloud cover along with a rising cloud-top height and thickening cloud depth moving downstream off the coasts (Figure 3, right). However, REF_amip (Figure 3, left) tends to overall underestimate the cloud amount through the cross sections. Specifically, REF_amip produces the cloud fraction much less near the coast and fails to simulate the elevated maxima prevalent in the

240   observed cross sections. This reflects the limitations of the HB turbulence scheme in simulating stratocumulus. In addition, REF_amip is prone to abruptly reduce the cloud amount out of the coastal stratocumulus regions, resulting in an almost cloudless state offshore. No clear transitional regime is simulated, which can be attributed to the excessive vertical mixing from the original Hack shallow convection scheme over the western edge of the stratocumulus regime. In contrast to REF_amip, the cross sections in NEW_amip depict a very different picture. With new configurations of boundary-layer

245   turbulence and shallow cumulus schemes, NEW_amip presents more realistic characteristics of subtropical Sc-to-Cu transition (Figure 3, middle). The qualitative aspects of the transition are better captured for all regions: most notably the

gradual reduction of cloud cover as it moves offshore and the placement of the maximum cloudiness which generally occurs somewhat offshore, as in GOCCP. A possible reason for the over-extension of Sc in NEW_amip may be that the decoupling criterion added to the Hack shallow convection scheme is too strong, leading to the weak vertical mixing over the eastern
250   edge of the shallow cumulus regime.

## 4 Alleviated double ITCZ in the coupled simulations

The underestimated stratus cloud cover in the SEP has long been recognized as a possible contributor to the double ITCZ bias in the eastern Pacific. The above-mentioned analysis from the atmosphere-only runs demonstrates that the simulated low-cloud amount in the SEP can be increased obviously by modifying parameterizations of BL turbulence and shallow
255   convection. Is it possible that the improved cloud simulation reduces the warm bias of SST in the SEP and hence helps to eliminate the double ITCZ bias? Below will clarity the effects of the increased low-cloud amount in the coupled simulations.

### 4.1 Precipitation

### 4.1.1 Precipitation patterns

Figure 4 shows simulated annual-mean precipitation distributions compared with the GPCP and CMAP observational
260   estimates. Two sets of observational estimates are presented here to illustrate the uncertainty in observations. In observations (Figure 4a and 4b), massive precipitation can be found in regions of Asian monsoon and midlatitude storm tracks over the northwest Pacific and Atlantic Oceans. In the tropics, the primary peaks are located in the eastern Indian Ocean and Maritime Continent regions. Furthermore, two zonal precipitation bands are located at $0° – 10°N$ in the equatorial Pacific and Atlantic oceans, respectively, constituting the northern ITCZ. The southern South Pacific convergence zone (SPCZ) is
265   mainly located around $5°S – 10°S$ near the western Pacific warm pool region and experiences a southeast tilt as it extends eastward into the central Pacific. In the southeast Pacific, the SPCZ, the west coast of South America, and the northern ITCZ bound a triangular-shaded dry region, which is dominated by stratocumulus and trade cumulus. While the main spatial patterns of observed precipitation climatology are properly reproduced, prominent double ITCZ biases develop in the simulation of tropical precipitation in REF_cmip (Figure 4c). Specifically, the simulated SPCZ does not tilt southeastward as
270   that in the observation but overly extends eastward, leading to the excessive precipitation in the central and eastern equatorial Pacific. The precipitation band of $> 3$ mm day$^{-1}$ between $10°S$ and $5°S$ extends as far east as $90°W$. Also, a spurious precipitation band appears in the southern Atlantic at $10°S – 0°$. In contrast, NEW_cmip significantly reduces the SPCZ bias in the central and eastern equatorial Pacific and produces no rain belt in the tropical southern Atlantic (Figure 4d). The precipitation of $> 3$ mm day$^{-1}$ between $10°S$ and $5°S$ is confined to west of $130°W$ in the Pacific Ocean.

### 4.1.2 Asymmetry of the tropical precipitation

The asymmetry in the meridional distribution of tropical precipitation is a characteristic in the observed ITCZ. Figure 5 shows the zonally averaged annual mean precipitation from the GPCP and CMAP observations, and the REF_cmip and NEW_cmip simulations. The CMAP observations generally show very similar latitudinal variations to that of GPCP, but with slightly stronger precipitation intensity. These two sets of observational estimates both show a pronounced asymmetry about the equator with strong northern ITCZ peak at 5° – 10°N and weak southern ITCZ peak at 10° – 5°S. The precipitation produced by REF_cmip is about 50% larger than the observed amounts in the southern ITCZ, which comes largely from the spurious rainfall in the central and eastern Pacific and Atlantic south of the equator. The precipitation rate in the southern ITCZ is comparable to that in the northern ITCZ, and the meridional distribution of the tropical precipitation tends to be symmetrical. In contrast, NEW_cmip produces much weaker precipitation in the southern ITCZ, which is in good agreement with the observed asymmetry.

To quantitatively examine the ITCZ fidelity in the coupled simulations, the tropical precipitation asymmetry index ($A_P$), which is defined as the precipitation difference between the northern (0° – 20°N) and southern (20°S – 0°) tropics normalized by the tropical mean, is calculated as follows (Hwang and Frierson, 2003; Xiang et al., 2017; Adam et al., 2018)

$$A_P = \left( \overline{P}_{0-20^\circ \text{N}} - \overline{P}_{20^\circ \text{S}-0} \right) \Big/ \overline{P}_{20^\circ \text{S}-20^\circ \text{N}} , \qquad (7)$$

where the overbar represents a zonal mean of precipitation. The observed annual mean $A_P$ is 0.194 in GPCP and 0.214 in CMAP, respectively, because the ITCZ is predominantly north of the equator. In the coupled simulations, the $A_P$ index increases from −0.024 in REF_cmip to 0.147 in NEW_cmip, which is much closer to the observed values, primarily because the southern ITCZ in the Pacific and Atlantic sectors is reduced.

### 4.1.3 Seasonal cycle of precipitation over eastern Pacific

Figure 6 presents the seasonal evolution of monthly precipitation averaged between 90°W and 160°W from the GPCP observations and coupled simulations. In the observation (Figure 6a), the precipitation greater than 3 mm day$^{-1}$ occurs only between March and April south of the equator, whereas the precipitation greater than 3 mm day$^{-1}$ persists throughout the year in the northern ITCZ region with higher precipitation rates occurring between April and November. The double ITCZ bias in REF_cmip comes mainly from overestimated precipitation as high as 12 mm day$^{-1}$ between 5°S and 10°S in boreal winter and spring (Figure 6b). In contrast, the excessive precipitation south of the equator in boreal winter and spring is reduced in NEW_cmip and closer to the observation although the maximum rainfall is slightly larger in April (Figure 6c and 6d), indicating the alleviated double ITCZ bias. In addition, the northern ITCZ dry bias in the boreal winter and spring is also alleviated and the northern precipitation band in boreal summer and autumn moves closer to the equator in NEW_cmip.

A southern ITCZ (SI) index, simply defined as the annual mean precipitation rate over southeastern Pacific (20°S – 0°, 90° – 160°W; Bellucci et al., 2010), is used to quantify the coupled model biases in a more objective way. The simulated SI index decreases from 3.46 mm day$^{-1}$ in REF_cmip to 2.51 mm day$^{-1}$ in NEW_cmip, closer to the observational values (1.36

mm day$^{-1}$ in GPCP and 1.66 mm day$^{-1}$ in CMAP). The following analysis will focus on the Pacific ocean to understand the impact of improved boundary-layer turbulence and shallow convection schemes on the simulated ITCZ.

### 4.2 SST and the heat flux into the ocean

310   The annual mean precipitation change is closely related to the SST change (Song and Zhang, 2016). Figure 7 shows the annual mean SST from the HadISST observation, the REF_cmip and NEW_cmip simulations, and their differences in the Pacific. The 30-year average of HadISST from 1971 to 2000 is used as the observed climatology, in which the warm SST corresponds to the northern ITCZ and SPCZ precipitation (Figure 7a). The SST from REF_cmip, featured by a stronger cold tongue extending excessively westward along the equator, is warmer than the HadISST between 5°S and 20°S in the central

315   and eastern Pacific. A band of cold SST bias down to −3 K between 5°S and 5°N across the Pacific can be clearly seen from the difference between them (Figure 7c). There is a conspicuous region of warm bias up to 2 K between 5°S and 20°S east of 150°W, which has been attributed to the underestimation of clouds in this region (e.g., Ma et al. 1996). It should be noted that this study compares the SST from pre-industrial simulations to the present-climate observations. Considering the global warming trend, the pre-industrial SST should be colder than the 20th century observations, suggesting that the cold bias in

320   cold tongue region may be overestimated and the warm bias in the central and eastern Pacific may be underestimated. When the new boundary-layer turbulence and shallow convection schemes are used, the simulated warm water is cooled down by up to 4 K in the SEP relative to the REF_cmip (Figure 7d).

The SST differences between the NEW_cmip and REF_cmip simulations are determined by both the net surface heat flux difference and ocean dynamic heat transport difference. The differences between NEW_cmip and REF_cmip runs for

325   the atmospheric forcing on SST via surface heat flux $\Delta Q_{atm}$ is composed of differences of shortwave radiation $\Delta Q_{SW}$, longwave radiation $\Delta Q_{LW}$, latent heat flux $\Delta Q_{LH}$, and sensible heat flux $\Delta Q_{SH}$:

$$\Delta Q_{atm} = \Delta Q_{SW} + \Delta Q_{LW} + \Delta Q_{LH} + \Delta Q_{SH} \ . \tag{8}$$

The contributions of these four components are presented in Figure 8. In the SEP, the net atmospheric heat flux at sea surface is reduced in NEW_cmip, contributing to the cooled water in these regions. Among the atmospheric radiative heat

330   flux components, the shortwave radiation is dominant, while the longwave radiation exerts a smaller and opposite effect. The latent heat flux is similar to the longwave radiative flux, and the sensible heat flux is negligible. Overall, the shortwave response explains most of net surface heat flux response in the SEP.

### 4.3 The Walker circulation and the surface wind stress

Changes in the simulated SSTs lead to changes in the simulated large-scale atmospheric circulation. The JRA-55 reanalysis

335   data shows descending motion east of 150°W, which corresponds to the rainless state in the eastern Pacific between 5°S and 10°S, and intense ascending motion west of the dateline, which corresponds to the notable precipitation in the SPCZ (Figure

9a). In REF_cmip (Figure 9b), the weaker downward motion is limited to the middle and upper troposphere east of 125°W. The stronger upward motion occurs in the middle and upper troposphere between 150°W and 135°W, and is extended eastward to 100°W in the lower troposphere. Both the strengthened large-scale ascending motion and the weakened

340   descending motion in the eastern part of the Walker circulation contribute to the excessive precipitation in the southern ITCZ region, resulting in the double ITCZ bias in REF_cmip. When the new boundary-layer turbulence and shallow convection schemes are used, the descending branch of the Walker circulation is better simulated in NEW_cmip (Figure 9c). Compared with REF_cmip, the upward motion in the low troposphere shrinks to 120°W in NEW_cmip. Furthermore, the downward motion in the middle and upper troposphere is enhanced and expanded westward to 140°W, making it in better agreement

345   with the JRA-55 reanalysis. The improved descending branch of the Walker circulation is consistent with the decrease of precipitation relative to REF_cmip.

Figure 10 shows the annual mean differences of surface wind stress vectors and magnitudes between the NEW_cmip and REF_cmip simulations. The modified boundary-layer turbulence and shallow convection schemes result in increased southeasterly winds off the west coast of South America. In addition, the difference between NEW_cmip and REF_cmip

350   clearly shows the strengthened southeasterly trade winds in the eastern Pacific between 5°S and 10°S, corresponding to the stronger descending branch of the Walker circulation in NEW_cmip.

### 4.4 Enhanced cold advection in the upper ocean

The enhanced Walker circulation and surface wind stress subsequently induce strengthened cold advection in the upper ocean. Figure 11 shows the longitude-depth cross section of zonal ocean current and temperature averaged over 5°S – 10°S

355   for the difference between NEW_cmip and REF_cmip. The enhanced westward ocean current over the whole zonal band helps transport cooler water from east to west in NEW_cmip.

### 5 Discussion

#### 5.1 The Sc-to-Cu transition

The relative contribution of the UWMT boundary-layer scheme and modified Hack shallow convection scheme in portraying

360   the Sc-to-Cu transition is further examined. Figure 12 presents the vertical cross sections of cloud fraction through the five main subtropical stratocumulus regions in the sensitivity experiments of UWMT_amip and mHack_amip. UWMT_amip reproduces the elevated cloudiness maxima, which can be expected from the applicability of the UWMT turbulence scheme in simulating stratocumulus, but still suffers from the rapid dissipating of cloud cover downstream off the coasts (Figure 12, left). On the contrary, mHack_amip produces the gradual reduction of cloud amount offshore but misses the elevated

365   cloudiness maxima, and constrains the cloud to a very low level (Figure 12, right). Neither UWMT_amip nor mHack_amip captures all the significant transition characteristics, indicating that the coupling between boundary-layer turbulence and shallow convection is important for an accurate simulation of the Sc-to-Cu transition.

In this study, introducing the decoupling criterion in the Hack scheme aims to better treat the transition between the stratocumulus regime and shallow cumulus regime. Regime-dependent parameterizations have limitations when representing 370 various cloud regimes and their transitions. Two classes of unified parameterizations of boundary-layer turbulence and shallow convection have been documented in the literature, known as the eddy diffusion mass flux (EDMF) approach (Siebesma et al., 2007; Pergaud et al., 2009; Hourdin et al., 2013), and the higher-order turbulence closure (HOC) approach (Bogenschutz et al., 2013; Guo et al., 2010, 2014). Effects of these greater unification of cloud parameterizations on the double ITCZ bias in CGCMs will be further explored in future work.

### 5.2 Robustness of the alleviated double ITCZ

More investigations on the role of boundary-layer turbulence and shallow convection schemes in the double ITCZ formation in different CGCMs are desired. For simplicity, the UWMT and modified Hack schemes are employed in the high-resolution Beijing Climate Center Climate System Model version 2 (BCC-CSM2-HR), which is largely different from BCC-CSM2-MR with respect to model physics and dynamics, to examine the robustness of the alleviated double ITCZ through improving 380 parameterizations of boundary-layer turbulence and shallow convection.

During the transition from BCC-CSM2-MR to BCC-CSM2-HR, the atmospheric component increased its horizontal resolution to T266 (~ 0.45°) with a higher model top, and the physics package was essentially updated, especially the deep convection scheme. Furthermore, the oceanic component was upgraded to the Modular Ocean Model version 5 (MOM5). However, BCC-CSM2-HR suffered from the double ITCZ syndrome until the UWMT and modified Hack schemes were 385 introduced. This suggests that the boundary-layer and shallow convection schemes contribute primarily to the double ITCZ bias in BCC-CSM2-HR. The tropical precipitation patterns simulated in BCC-CSM2-HR barely manifest a double ITCZ, as shown in Figure 13. The triangular-shaded dry region in the SEP reproduced by BCC-CSM2-HR resembles the observed much better than that simulated in BCC-CSM2-MR, probably due to the improved interactions among the boundary-layer turbulence, shallow convection, and other processes. Anyway, improving parameterizations of boundary-layer turbulence 390 and shallow convection shows robustness in mitigating the double ITCZ syndrome in different models of BCC-CSM2-MR and BCC-CSM2-HR.

### 6 Summary and conclusions

It is a challenge to eliminate the double ITCZ problem, one of the most prominent systematic biases in CGCMs. This study investigates the roles of BL turbulence and shallow convection parameterizations in alleviating the double ITCZ bias using 395 the BCC-CSM2-MR. The original BCC-CSM2-MR presents a serious double ITCZ problem in precipitation, with two significant zonal rain bands straddling the equator across the Pacific. In contrast, the revised BCC-CSM2-MR with new configurations of BL turbulence and shallow convection schemes remarkably alleviates the spurious southern ITCZ bias associated with SST warm bias in the SEP, owing to the reduced net surface shortwave radiation associated with the

increased low cloud fraction. Correspondingly, the cooler water in the SEP induces stronger and wider subsiding motion of
400 the Walker circulation. The stronger Walker circulation and enhanced eastward surface wind stress in turn lead to increased
oceanic zonal cold advection from east to west in the southern equatorial Pacific.

Consistent with previous studies (Ma et al., 1996; Yu and Mechoso, 1999; Dai et al., 2003, 2005; Qin and Lin, 2018),
this study emphasizes the importance of stratus clouds and SSTs in the SEP in alleviating the double ITCZ bias via changes
in the tropical circulation and ocean dynamics. However, different with studies with modifications of cloud scheme itself,
405 this study focuses on the roles of BL turbulence and shallow convection in the low-level cloud simulation, and the
subsequent impacts on the mitigation of the double ITCZ. It is found that the simulated low clouds are sensitive to both BL
turbulence and shallow convection parameterizations. Better consistency between the BL turbulence scheme and the shallow
convection scheme results in better simulation of the Sc-to-Cu transition. In conclusion, this study indicates that improving
parameterizations of BL turbulence and shallow convection is an effective way to reduce the double ITCZ in CGCMs.

410 In the present study, the alleviation of the double ITCZ problem is accompanied by an amplification of the cold tongue
bias, as found by many early efforts focusing on the role of low clouds. The inverse responses of the double ITCZ and cold
tough biases to southeast Pacific low clouds suggest that other parameterized processes, e.g., deep convection, may play an
important role in the accurate simulation of the ITCZ-cold tongue complex. Song and Zhang (2018) demonstrated that the
double ITCZ bias is largely eliminated and the cold bias in equatorial cold tongue is also significantly reduced through
415 modifying the deep convection scheme in the Community Earth System Model version 1.2.1 (CESM1.2.1). The effect of
improving the representation of deep convection on the double ITCZ bias in BCC-CSM2-MR is beyond the scope of this
paper and will be explored in future work.

*Code and data availability*. Please contact the corresponding author if readers want to validate the model modifications and
420 to conduct replication experiments. The source codes and required input data of the BCC models are freely available upon
request from Tongwen Wu (twwu@cma.gov.cn).

*Author contributions*. YL modified the source codes, designed and performed all the experiments presented in the paper, and
wrote a large part of the paper. TW supervised the BCC-CSM development and provided critical comments on the paper. All
425 the authors continuously discussed the model development and the results.

*Competing interests*. The authors declare that they have no conflict of interest.

*Acknowledgements*. This work was supported by The National Key Research and Development Program of China (2016YFA
430 0602100). We gratefully acknowledge the groups of GPCP (https://www.esrl.noaa.gov/psd/data/gridded/data.gpcp.html), C
MAP (https://www.esrl.noaa.gov/psd/data/gridded/data.cmap.html), CALIPSO-GOCCP (http://climserv.ipsl.polytechnique.f
r/cfmip-obs), CERES-EBAF (https://ceres.larc.nasa.gov/products.php?product=EBAF-Product), HadISST (https://www.met

office.gov.uk/hadobs/hadisst), and the JRA-55 reanalysis (https://jra.kishou.go.jp/JRA-55) for providing public access to various observational data sets. All the graphics in this study are created by the NCAR Command Language (NCL; doi:10.5065/D6WD3XH5).

435

**References**

Adam, O., Schneider, T., and Brient, F.: Regional and seasonal variations of the double-ITCZ bias in CMIP5 models, Clim. Dynam., 51, 101-117, doi:10.1007/s00382-017-3909-1, 2018.

440 Adler, R. F., Huffman, G. J., Chang, A., Ferraro, R., Xie, P., Janowiak, J., Rudolf, B., Schneider, U., Curtis, S., Bolvin, D., Gruber, A., Susskind, J., and Arkin, P.: The version 2 Global Precipitation Climatology Project (GPCP) monthly precipitation analysis (1979-present), J. Hydrometeor., 4, 1147-1167, 2003.

Bellucci, A., Gualdi, S., and Navarra, A.: The double-ITCZ syndrome in coupled general circulation models: The role of large-scale vertical circulation regimes, J. Climate, 23, 1127-1145, doi:10.1175/2009JCLI3002.1, 2010.

445 Bodas-Salcedo, A., Webb, M. J., Bony, S., Chepfer, H., Dufresne, J. L., Klein, S. A., Zhang, Y., Marchand, R., Haynes, J. M., Pincus, R., and John, V. O.: COSP: Satellite simulation software for model assessment, B. Am. Meteorol. Soc., 92, 1023, doi:10.1175/2011BAMS2856.1, 2011.

Bogenschutz, P. A., Gettelman, A., Morrison, H., Larson, V. E., Craig, C., and Schanen, D. P.: Higher-order turbulence closure and its impact on climate simulations in the Community Atmosphere Model, J. Climate, 26, 9655-9676, 2013.

450 Bretherton, C. S. and Park, S.: A new moist turbulence parameterization in the Community Atmosphere Model, J. Climate, 22, 3422-3448, 2009.

Bretherton, C. S. and Wyant, M. C.: Moisture transport, lower tropospheric stability, and decoupling of cloud-topped boundary layers, J. Atmos. Sci., 54, 148-167, 1997.

Chepfer, H., Bony, S., Winker, D., Cesana, G., Dufresne, J. L., Minnis, P., Stubenrauch, J., and Zeng, S.: The GCM-oriented
455 CALIPSO cloud product (CALIPSO-GOCCP), J. Geophys. Res., 115, D00H16, doi:10.1029/2009JD012251, 2010.

Dai, F., Yu, R., Zhang, X., Yu, Y., and Li, J.: The impact of low-level cloud over the eastern subtropical Pacific on the "double ITCZ" in LASG FGCM-0, Adv. Atmos. Sci., 20, 461-474, doi:10.1007/BF02690804, 2003.

Dai, F., Yu, R., Zhang, X., and Yu, Y.: Impacts of an improved low-level cloud scheme on the eastern Pacific ITCZ-cold tongue complex, Adv. Atmos. Sci., 22, 559-574, doi:10.1007/BF02918488, 2005.

460 Griffies, S. M., Gnanadesikan, A., Dixon, K. W., Dunne, J. P., Gerdes, R., Harrison, M. J., Rosati, A., Russell, J. L., Samuels, B. L., Spelman, M. J., Winton, M., and Zhang, R.: Formulation of an ocean model for global climate simulations, Ocean Sci., 1, 45-79, doi:10.5194/os-1-45-2005, 2005.

Guo, H., Golaz, J.-C., Donner, L. J., Larson, V. E., Schanen, D. P., and Griffin, B. M.: Multi-variate probability density functions with dynamics for cloud droplet activation in large-scale models: Single column tests, Geosci. Model Dev., 3,
465      475-486, 2010.

Guo, H., Golaz, J.-C., Donner, L. J., Ginoux, P. A., and Hemler, R. S.: Multi-variate probability density functions with dynamics in the GFDL atmospheric general circulation model: Global tests, J. Climate, 27, 2087-2108, doi:10.1175/JCLI-D-13-00347.1, 2014.

Hack, J. J.: Parameterization of moist convection in the National Center for Atmospheric Research Community Climate
470      Model (CCM2), J. Geophys. Res., 99, 5551-5568, 1994.

Holtslag, A. A. M. and Boville, B. A.: Local versus nonlocal boundary-layer diffusion in a glocal climate model, J. Climate, 6, 1825-1842, 1993.

Hourdin, F., Grandpeix, J.-Y., Rio, C., Bony, S., Jam, A., Cheruy, F., Rochetin, N., Fairhead, L., Idelkadi, A., Musat, I., Dufresne, J.-L., Lahellec, A., Lefebvre, M.-P., and Roehrig, R.: LMDZ5B: the atmospheric component of the IPSL
475      climate model with revisited parameterizations for clouds and convection, Clim. Dynam., 40, 2193-2222, doi:10.1007/s00382-012-1343-y, 2013.

Hwang, Y.-T. and Frierson, D. M. M.: Link between the double-intertropical convergence zone problem and cloud biases over the Southern Ocean, Proc. Natl. Acad. Sci. USA, 110, 4935-4940, doi:10.1073/pnas.1213302110, 2013.

Kay, J. E., Yettella, V., Medeiros, B., Hannay, C., and Cadwell, P.: Global climate impacts of fixing the Southern Ocean
480      shortwave radiation bias in the Community Earth System Model (CESM), J. Climate, 29, 4617-4636, doi:10.1175/JCLI-D-15-0358.1, 2016.

Klein, S. A. and Hartmann, D. L.: The seasonal cycle of low stratiform cloud, J. Climate, 6, 1587-1606, 1993.

Kobayashi, S., Ota, Y., Harada, Y., Ebita, A., Moriya, M., Onoda, H., Onogi, K., Kamahori, H., Kobayashi, C., Endo, H., Miyaoka, K., and Takahashi, K.: The JRA-55 reanalysis: General specifications and basic characteristics, J. Meteorol.
485      Soc. Jpn., 93, 5-48, doi:10.2151/jmsj.2015-001, 2015.

Large, W. G. and Danabasoglu, G.: Attribution and impacts of upper-ocean biases in CCSM3, J. Climate, 19, 2325-2346, doi:10.1175/JCLI3740.1, 2006.

Li, G. and Xie S.-P.: Tropical biases in CMIP5 multimodel ensemble: The excessive equatorial Pacific cold tongue and double ITCZ problems, J. Climate, 27, 1765-1780, doi:10.1175/JCLI-D-13-00337.1, 2014.

490 Li, W., Zhang, Y., Shi, X., Zhou, W., Huang, A., Mu, M., Qiu, B., and Ji, J.: Development of land surface model BCC_AVIM2.0 and its preliminary performance in LS3MIP/CMIP6, J. Meteor. Res., 33, 851-869, doi:10.1007/s13351-019-9016-y, 2019.

Lin, J.-L.: The double-ITCZ problem in IPCC AR4 coupled GCMs: Ocean-atmosphere feedback analysis, J. Climate, 20, 4497-4525, doi:10.1175/JCLI4272.1, 2007.

495 Liu, H., Zhang, M., and Lin, W.: An investigation of the initial development of the double-ITCZ warm biases in the CCSM, J. Climate, 25, 140-155, doi:10.1175/2011JCLI4001.1, 2012.

Loeb, N. G., Doelling, D. R., Wang, H., Su, W., Nguyen, C., Corbett, J. G., Liang, L., Mitrescu, C., Rose, F. G., and Kato, S.: Clouds and the Earth's Radiant Energy System (CERES) Energy Balanced and Filled (EBAF) Top-of-Atmosphere (TOA) edition-4.0 data product, J. Climate, 31, 895-918, doi:10.1175/JCLI-D-17-0208.1, 2018.

500 Lu, Y., Zhou, M., and Wu, T.: Validation of parameterizations for the surface turbulent fluxes over sea ice with CHINARE 2010 and SHEBA data, Polar Res., 32, 20818, doi:10.3402/polar.v32i0.20818, 2013.

Lu, Y., Wu, T., Jie, W., Scaife, A. A., Andrews, M. B., and Richter, J. H.: Variability of the stratospheric quasi-biennial oscillation and its wave forcing simulated in the Beijing Climate Center Atmospheric General Circulation Model, J. Atmos. Sci., 77, 149-165, doi:10.1175/JAS-D-19-0123.1, 2020.

505 Ma, C.-C., Mechoso, C. R., Robertson, A. W., and Arakawa, A.: Peruvian stratus clouds and the tropical Pacific circulation: A coupled ocean-atmosphere GCM study, J. Climate, 9, 1635-1645, doi:10.1175/1520-0442(1996)009<1635:PSCATT>2.0.CO;2, 1996.

Manganello, J. V. and Huang B.: The influence of systematic errors in the Southeast Pacific on ENSO variability and prediction in a coupled GCM, Clim. Dynam., 32, 1015-1034, doi:10.1007/s00382-008-0407-5, 2009.

510 Mechoso, C. R., Robertson, A. W., Barth, N., Davey, M. K., Delecluse, P., Gent, P. R., Ineson, S., Kirtman, B., Latif, M., Le Treut, H., Nagai, T., Neelin, J. D., Philander, S. G. H., Polcher, J., Schopf, P. S., Stockdale, T., Suarez, M. J., Terray, L., Thual, O., and Tribbia, J. J.: The seasonal cycle over the tropical Pacific in coupled ocean-atmosphere general circulation models, Mon. Weather Rev., 123(9), 2825-2838, doi:10.1175/1520-0493(1995)123<2825:TSCOTT>2.0.CO;2, 1995.

515 Pergaud, J., Masson, V., Malardel, S., and Couvreux, F.: A parameterization of dry thermals and shallow cumuli for mesoscale numerical weather prediction, Bound.-Layer Meteor., 132, 83-106, 2009.

Qin, Y. and Lin, Y.: Alleviated double ITCZ problem in the NCAR CESM1: A new cloud scheme and the working mechanisms, J. Adv. Model. Earth Syst., 10, doi:10.1029/2018MS001343, 2018.

Rayner, N. A.: Global analyses of sea surface temperature, sea ice, and night marine air temperature since the late nineteenth
520 century, J. Geophy. Res., 108, 4407, doi:10.1029/2002JD002670, 2003.

Schneider, E. K., Fennessy, M. J., and Kinter, J. L. I.: A statistical-dynamical estimate of winter ENSO teleconnections in a future climate, J. Climate, 22, 6624-6638, doi:10.1175/2009JCLI3147.1, 2009.

Siebesma, A. P., Soares, P. M. M., and Teixeira, J.: A combined eddy-diffusivity mass-flux approach for the convective boundary layer, J. Atmos. Sci., 64, 1230-1248, 2007.

525 Song, F. and Zhang, G. J.: Effects of southeastern Pacific sea surface temperature on the double-ITCZ bias in NCAR CESM1, J. Climate, 29, 7417-7433, doi:10.1175/JCLI-D-15-0852.1, 2016.

Song, X. and Zhang, G. J.: Convection parameterization, tropical Pacific double ITCZ, and upper-ocean biases in the NCAR CCSM3. Part I: Climatology and atmospheric feedback, J. Climate, 22, 4299-4315, doi:10.1175/2009JCLI2642.1, 2009.

Song, X. and Zhang, G. J.: The roles of convection parameterization in the formation of double ITCZ syndrome in the
530 NCAR CESM: I. Atmospheric processes, J. Adv. Model. Earth Syst., 10, doi:10.1002/2017MS001191, 2018.

Turton, J. D. and Nicholls, L.: A study of the diurnal variation of stratocumulus using a multiple mixed-layer model, Q. J. R. Meteorol. Soc., 113, 969-1009, 1987.

Williams, K. D., Copsey, D., Blockley, E. W., Bodas-Salcedo, A., Calvert, D., Comer, R., Davis, P., Graham, T., Hewitt, H. T., Hill, R., Hyder, P., Ineson, S., Johns, T. C., Keen, A. B., Lee, R. W., Megann, A., Milton, S. F., Rae, J. G. L.,
535      Roberts, M. J., Scaife, A. A., Schiemann, R., Storkey, D., Thorpe, L., Watterson, I. G., Walters, D. N., West, A., Wood, R. A., Woollings, T., and Xavier, P. K.: The Met Office Global Coupled model 3.0 and 3.1 (GC3.0 and GC3.1) configurations, J. Adv. Model. Earth Syst., 10, 357-380, doi:10.1002/2017MS001115, 2018.

Willton, M.: A reformulated three-layer sea ice model, J. Atmos. Ocean. Tech., 17, 525-531, 2000.

Woelfle, M. D., Bretherton, C. S., Hannay, C., and Neale, R.: Evolution of the double-ITCZ bias through CESM2
540      development, J. Adv. Model. Earth Syst., 11, 1873-1893, doi:10.1029/2019MS001647, 2019.

Wood, R. and Bretherton, C. S.: Boundary-layer depth, entrainment, and decoupling in the cloud-capped subtropical and tropical marine boundary layer, J. Climate, 17, 3576-3588, 2004.

Wu, T.: A mass-flux cumulus parameterization scheme for large-scale models: Description and test with observations, Clim. Dynam., 38, 725-744, doi:10.1007/s00382-011-0995-3, 2012.

545   Wu, T., Lu, Y., Fang, Y., Xin, X., Li, L., Li, W., Jie, W., Zhang, J., Liu, Y., Zhang, L., Zhang, F., Zhang, Y., Wu, F., Li, J., Chu, M., Wang, Z., Shi, X., Liu, X., Wei, M., Huang, A., Zhang, Y., and Liu, X.: The Beijing Climate Center Climate System Model (BCC-CSM): the main progress from CMIP5 to CMIP6, Geosci. Model Dev., 12, 1573-1600, doi:10.5194/gmd-12-1573-2019, 2019.

Wu, T., Yu, R., and Zhang, F.: A modified dynamic framework for atmospheric spectral model and its application, J. Atmos.
550      Sci., 65, 2235-2253, 2008.

Wu, T., Yu, R., Zhang, F., Wang, Z., Dong, M., Wang, L., Jin, X., Chen, D. L., and Li, L.: The Beijing Climate Center atmospheric general circulation model: description and its performance for the present-day climate, Clim. Dynam., 34, 123-147, doi:10.1007/s00382-008-0487-2, 2010.

Xiang, B., Zhao, M., Held, I. M., and Golaz, J. C.: Predicting the severity of spurious "double ITCZ" problem in CMIP5
555      coupled models from AMIP simulations. Geophys. Res. Lett., 44, 1520-1527, doi:10.1002/2016GL071992, 2017.

Xie, P. and Arkin, P. A.: Global precipitation: A 17-year monthly analysis based on gauge observations, satellite estimates, and numerical model outputs, Bull. Amer. Meteor. Soc., 78, 2539-2558, 1997.

Yu, J.-Y. and Mechoso, C. R.: Links between annual variations of Peruvian stratocumulus clouds and of SST in the eastern equatorial Pacific, J. Climate, 12, 3305-3318, doi:10.1175/1520-0442(1999)012<3305:LBAVOP>2.0.CO;2, 1999.

560   Zhang, G. J. and Song, X.: Convection parameterization, tropical Pacific double ITCZ, and upper-ocean biases in the NCAR CCSM3. Part II: Coupled feedback and the role of ocean heat transport, J. Climate, 23, 800-812, doi:10.1175/2009JCLI3109.1, 2010.

Zhang, G. J., Song, X., and Wang, Y.: The double ITCZ syndrome in GCMs: A coupled feedback problem among convection, clouds, atmospheric and ocean circulations, Atmos. Res., 229, 255-268, doi:10.1016/j.atmosres.2019.06.023, 2019.

Zhang, X., Liu, H., and Zhang, M.: Double ITCZ in coupled ocean-atmosphere models: from CMIP3 to CMIP5, Geophys. Res. Lett., 42, 8651–8659, doi:10.1002/2015GL065973, 2015.

Zuidema, P., Chang, P., Medeiros, B., Kirtman, B. P., Mechoso, R., Schneider, E. K., Toniazzo, T., Richter, I., Small, R. J., Bellomo, K., Brandt, P., de Szoeke, S., Farrar, J. T., Jung, E., Kato, S., Li, M., Patricola, C. M., Wang, Z., Wood, R., and Xu, Z.: Challenges and prospects for reducing coupled climate model SST biases in the eastern tropical Atlantic and Pacific oceans: The U.S. CLIVAR eastern tropical oceans synthesis working group, B. Am. Meterol. Soc., 97, 2305-2328, doi:10.1175/BAMS-D-15-00274.1, 2016.

**Table 1.** Summary of experimental setups.

| Run name | Boundary layer scheme | Shallow convection scheme |
|---|---|---|
| REF_amip | HB | Hack |
| NEW_amip | UWMT | modified Hack |
| REF_cmip | HB | Hack |
| NEW_cmip | UWMT | modified Hack |
| UWMT_amip | UWMT | Hack |
| mHack_amip | HB | modified Hack |

575
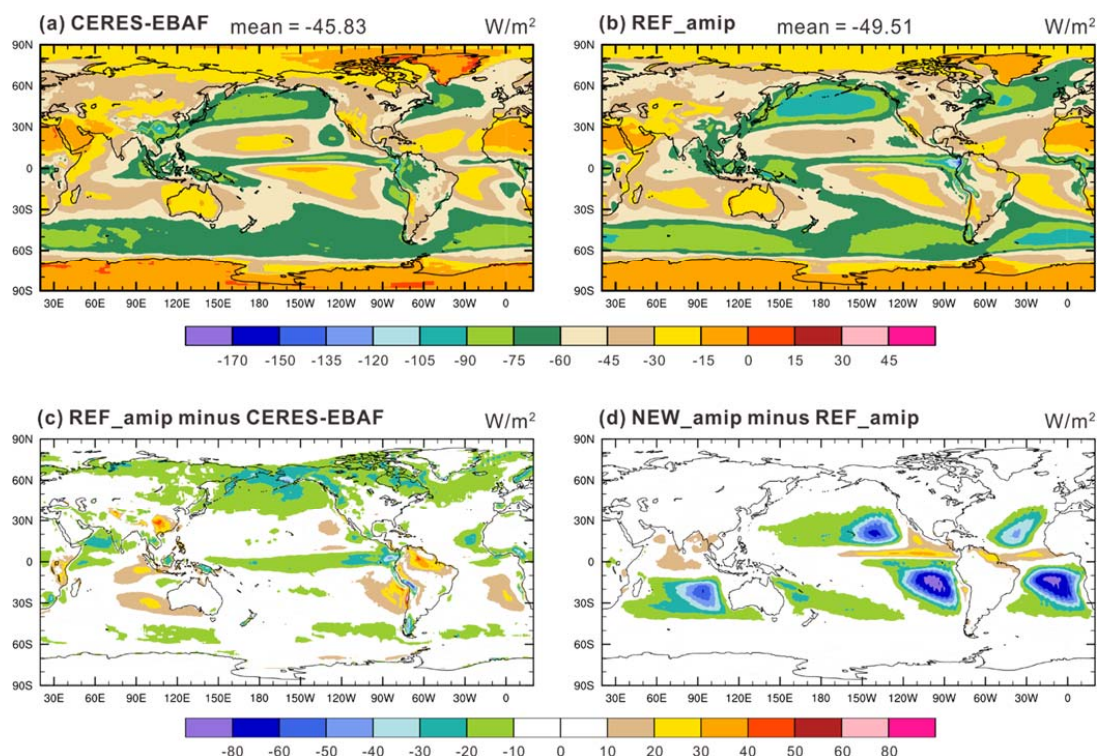
**Figure 1.** Annual mean climatologies of TOA SWCRF (W m$^{-2}$) from (a) CERES-EBAF observations (from 2001 to 2010), (b) REF_amip, and the differences between (c) REF_amip and observations, (d) NEW_amip and REF_amip. Shown atop panels (a) and (b) are global mean values.

580
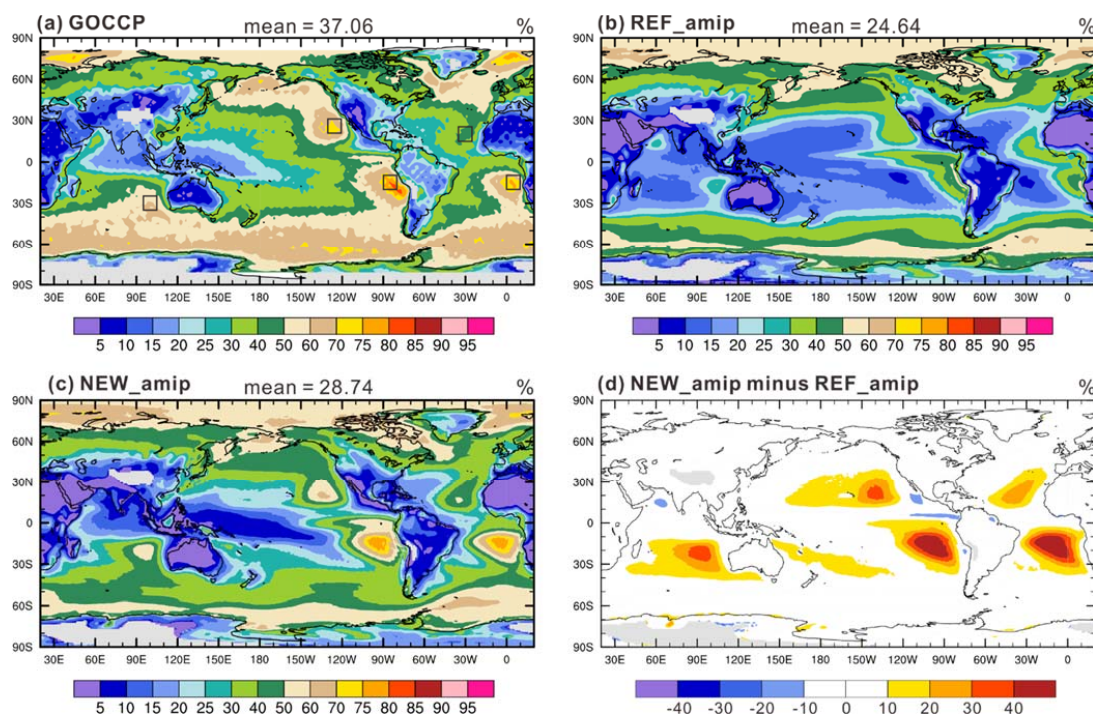
**Figure 2.** Annual mean low-level cloud fraction (%) from (a) GOCCP (from 2007 to 2012), (b) REF_amip, (c) NEW_amip, and (d) the difference between NEW_amip and REF_amip. Shown atop panels (a), (b) and (c) are global mean values. Boxes in panel (a) indicate the five main subtropical marine stratocumulus regions, namely, Peru (10°-20°S, 80°-90°W), California (20°-30°N, 120°-130°W), Australia (25°-35°S, 95°-105°E), Namibia (10°-20°S, 0°-10°E), and Canaria (15°-25°N, 25°-35°W).
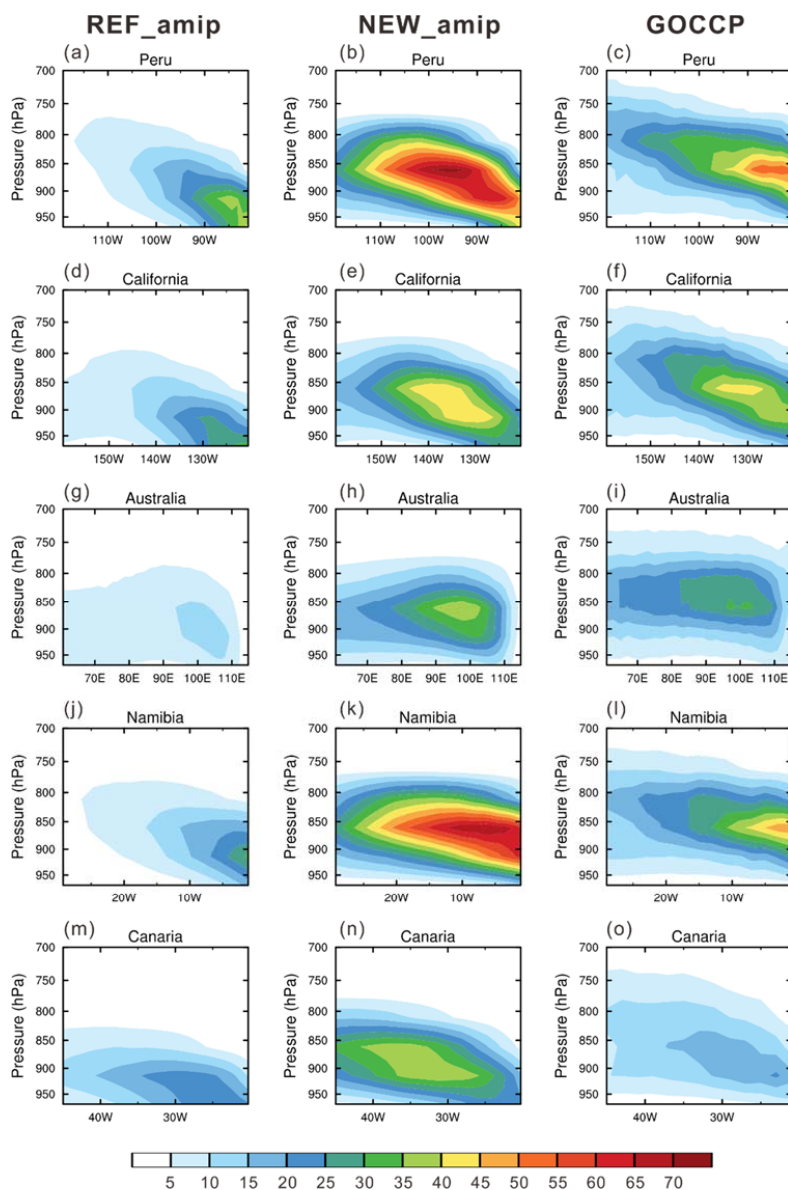
**Figure 3.** Cross sections of cloud fraction from five locations for (left) REF_amip, (center) NEW_amip, and (right) GOCCP. Refer to the boxes in Fig. 2 for the locations of the cross sections.
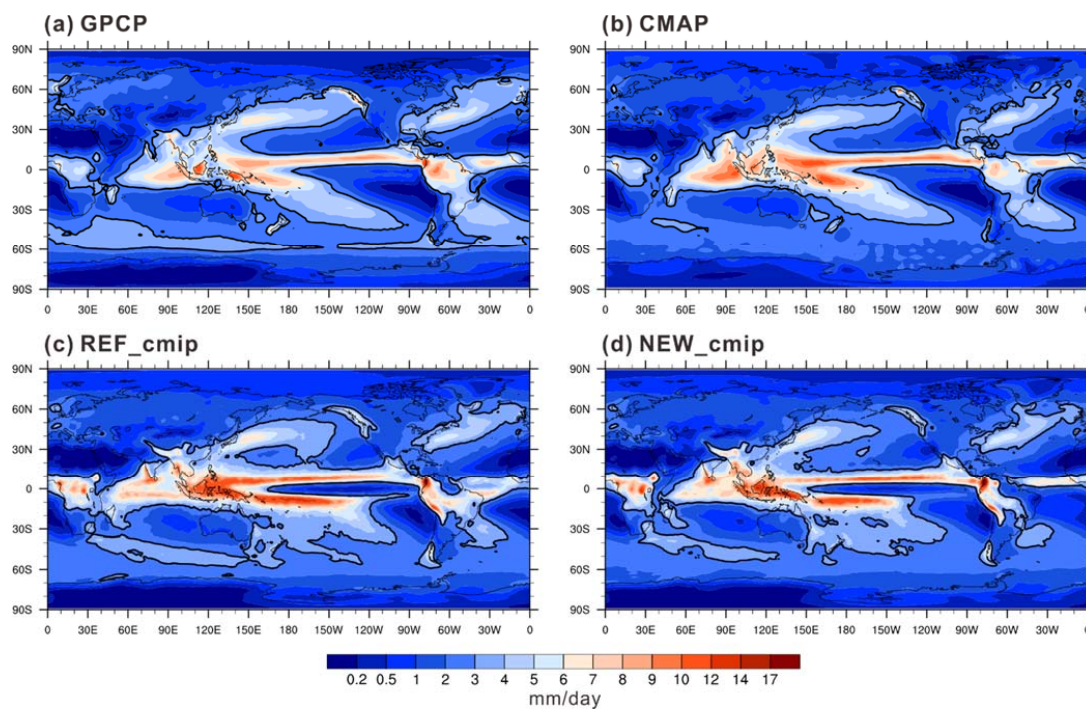
**Figure 4.** Annual mean precipitation rate (mm day$^{-1}$) from (a) GPCP, (b) CMAP, (c) REF_cmip, and (d) NEW_cmip. The 3 mm day$^{-1}$ contour is included in bold for reference.

595
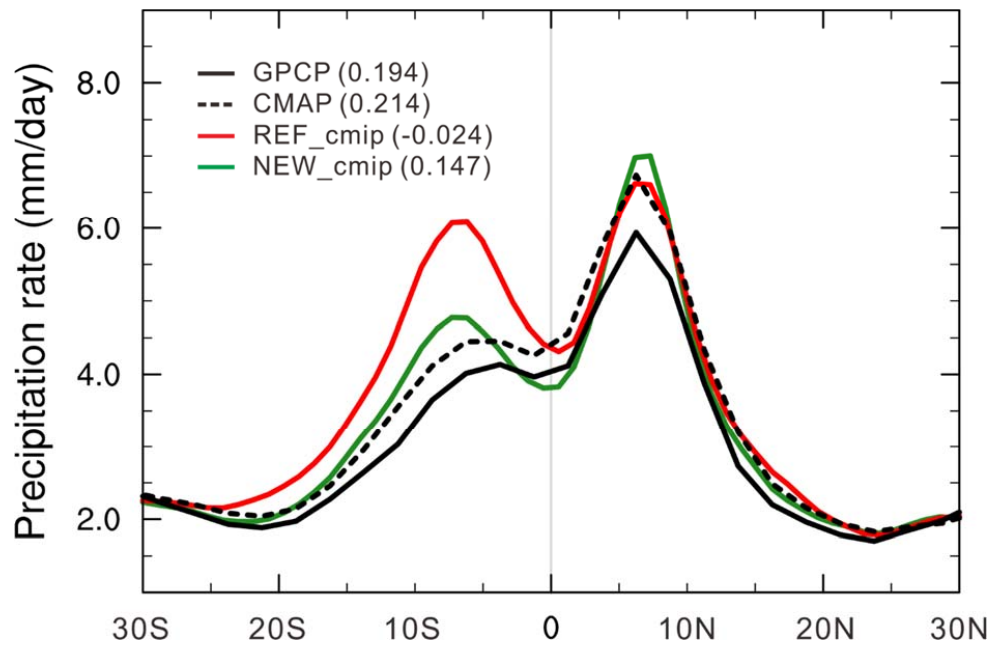
**Figure 5.** Zonal mean precipitation rate (mm day$^{-1}$) from GPCP, CMAP, REF_cmip and NEW_cmip in the tropics. Values of the tropical precipitation asymmetry index are indicated in parentheses.

600
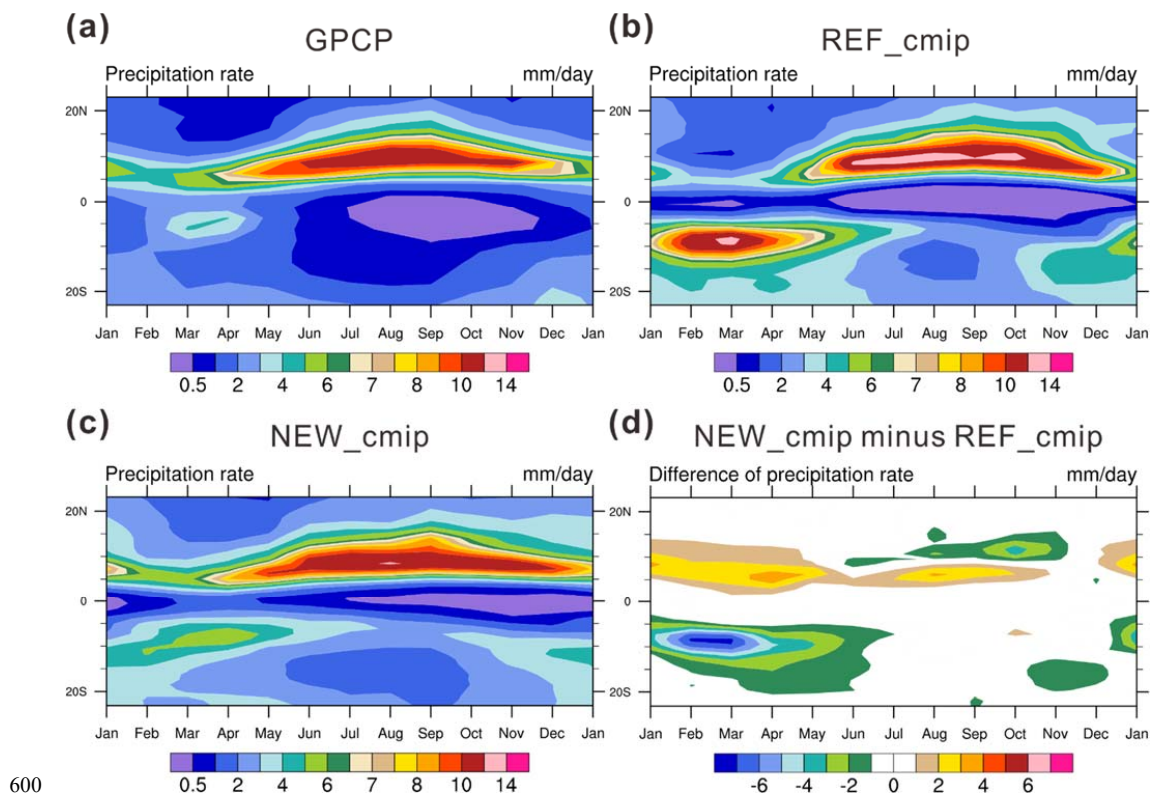
**Figure 6.** Seasonal cycle of precipitation rate (mm day$^{-1}$) averaged over eastern Pacific (90° - 160°W) for (a) GPCP, (b) REF_cmip, (c) NEW_cmip, and (d) the difference between NEW_cmip and REF_cmip.
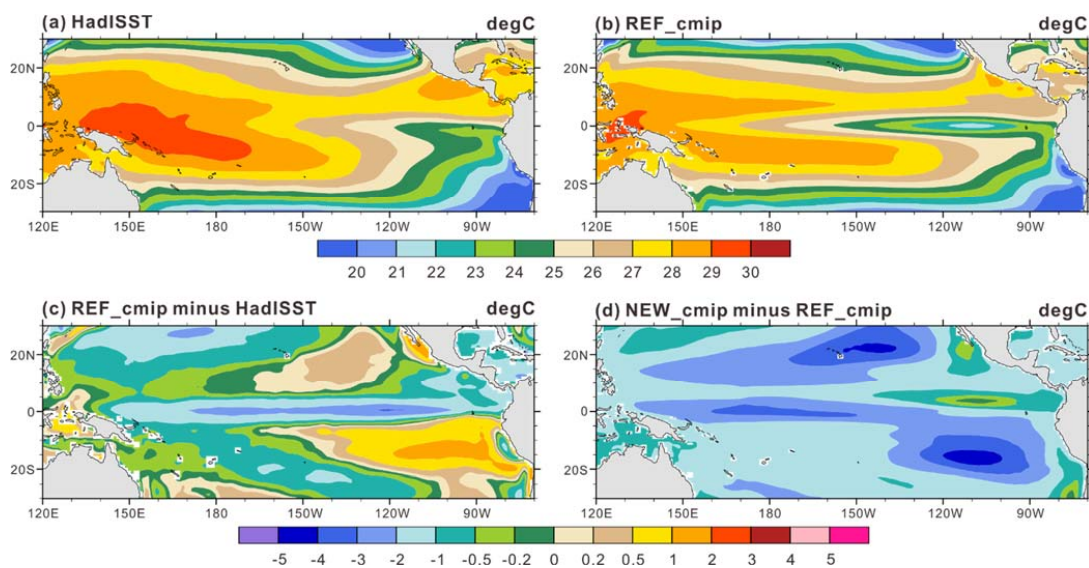
605 **Figure 7.** Annual mean sea surface temperature (°C) from (a) HadISST, and (b) REF_cmip, and the difference between (c) REF_cmip and HadISST, and (d) NEW_cmip and REF_cmip.
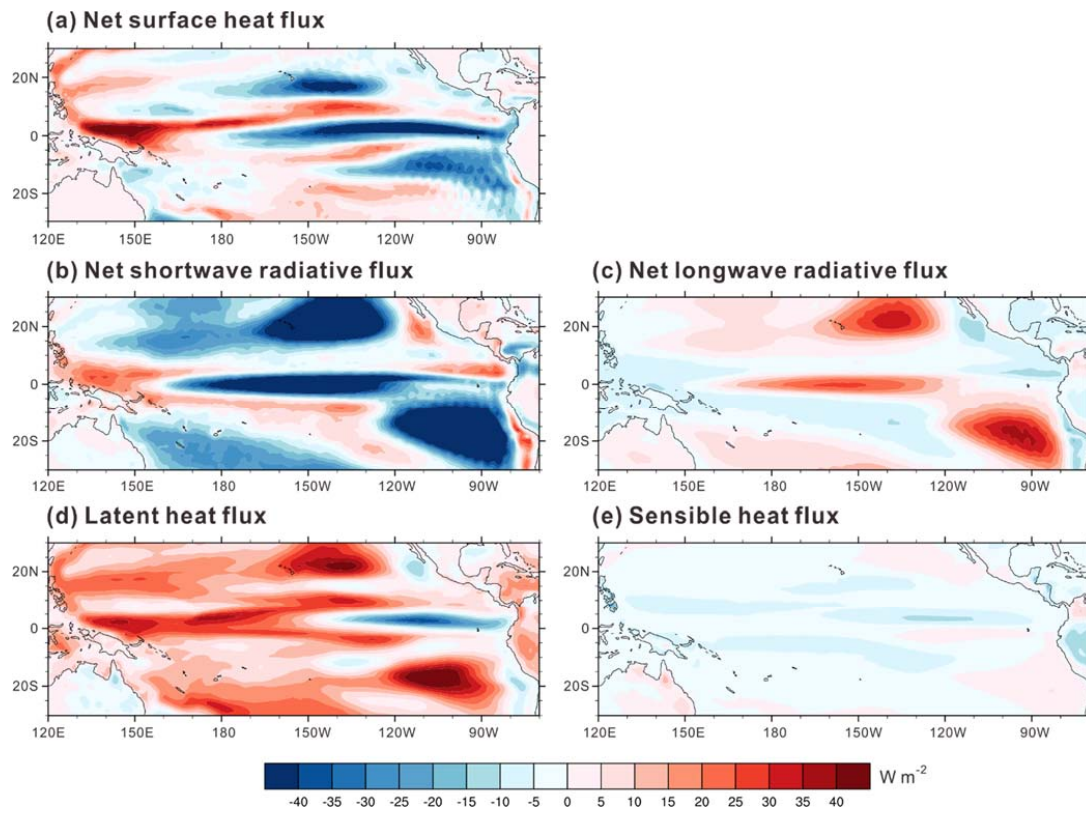
**Figure 8.** The differences between the NEW_cmip and REF_cmip simulations (W m$^{-2}$) for (a) net surface heat flux $\Delta Q_{atm}$, (b) net shortwave radiative flux $\Delta Q_{SW}$, (c) net longwave radiative flux $\Delta Q_{LW}$, (d) latent heat flux $\Delta Q_{LH}$, and (e) sensible heat flux $\Delta Q_{SH}$.
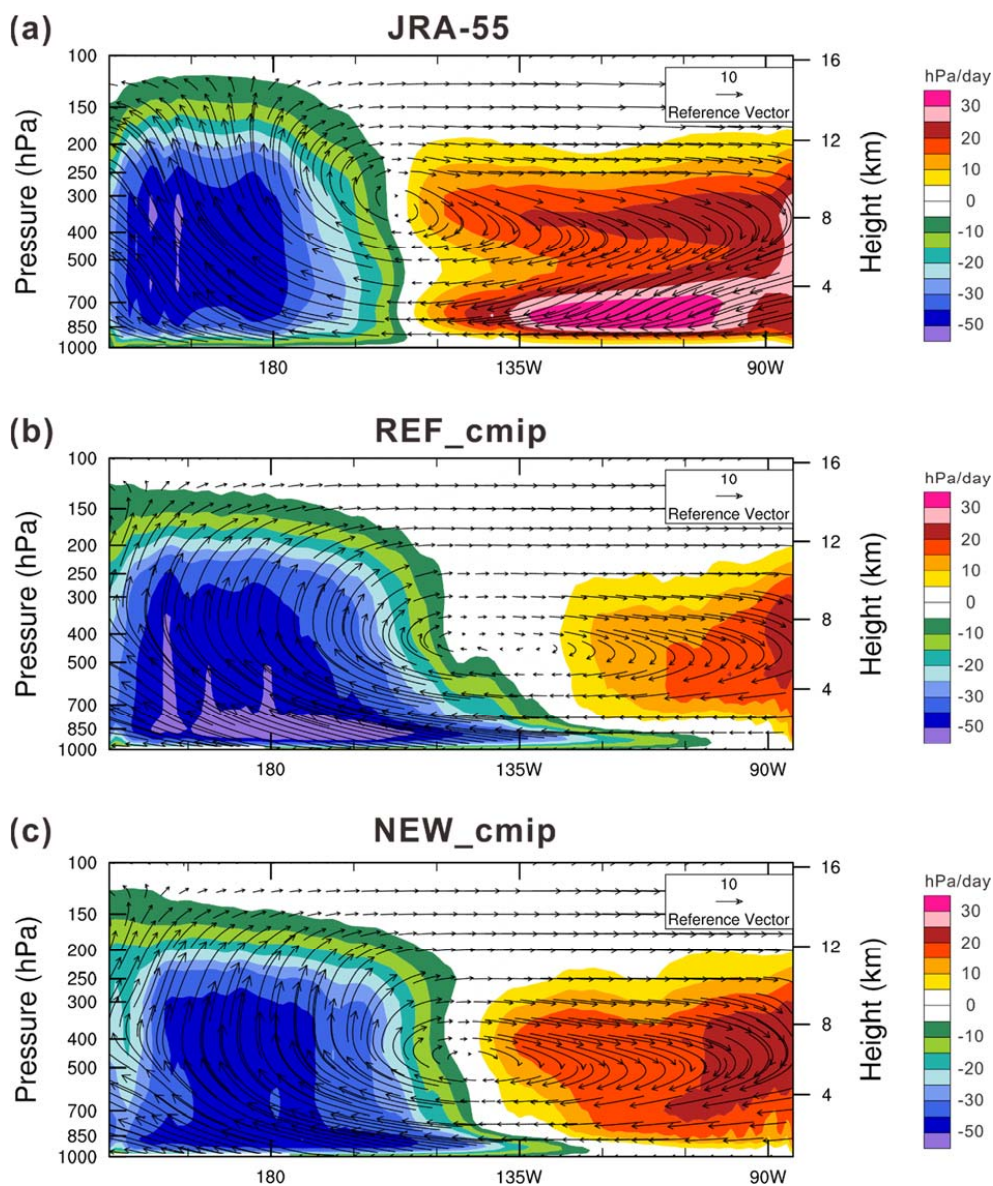
**Figure 9.** Annual mean vertical pressure velocity (hPa day$^{-1}$; shaded) and wind vectors (arrows) in the longitude-height cross section averaged over 5°S – 10°S for (a) the JRA-55 reanalysis, (b) REF_cmip, and (c) NEW_cmip.

615
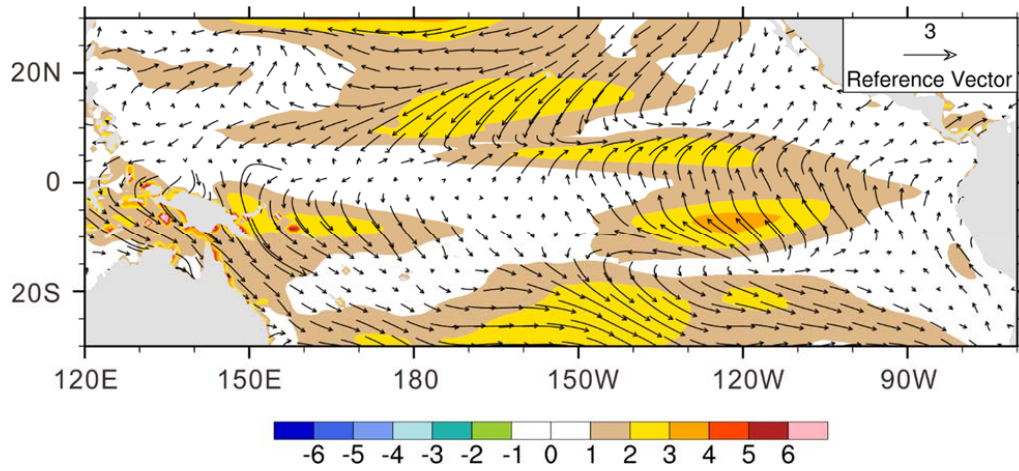
**Figure 10.** The difference of annual mean wind stress vector and wind stress magnitude (shaded, $10^{-2}$ N m$^{-2}$) between NEW_cmip and REF_cmip.
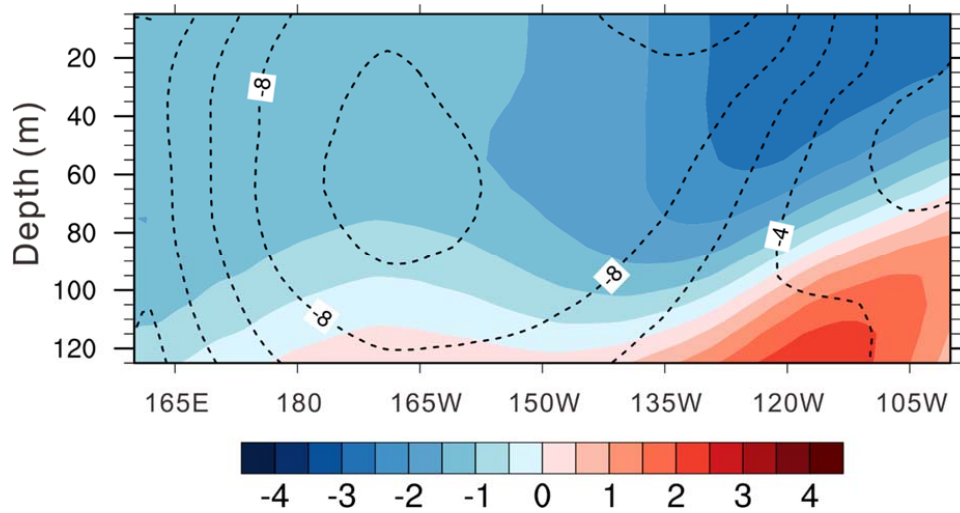
620

**Figure 11.** Longitude-depth cross section of zonal ocean current (contours; cm s$^{-1}$) and temperature (shaded; °C) averaged over over 5°S – 10°S for the difference between NEW_cmip and REF_cmip.
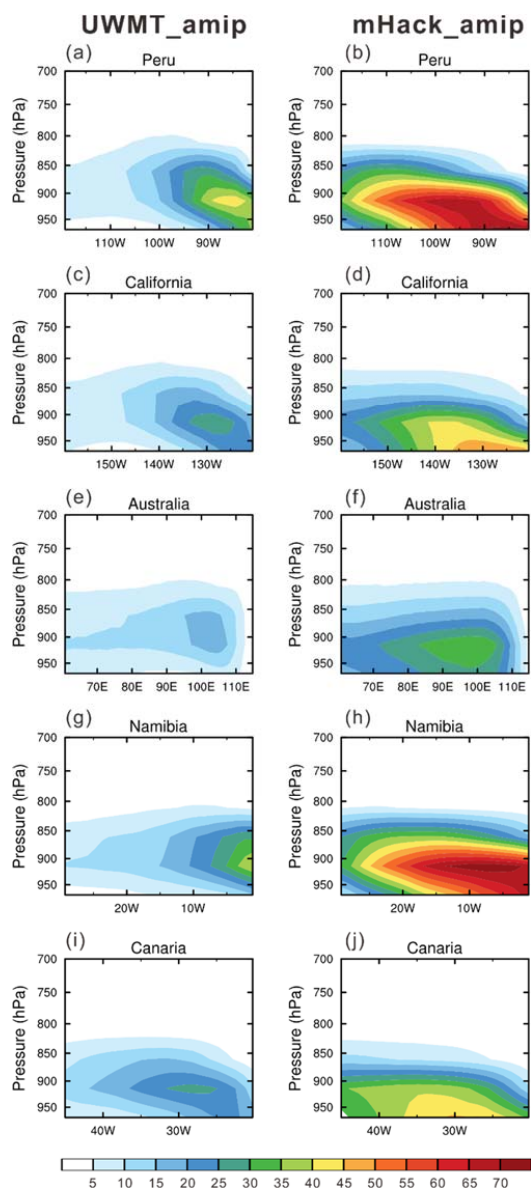
**Figure 12.** Cross sections of cloud fraction from five locations for (left) UWMT_amip, and (right) mHack_amip. Refer to the boxes in Fig. 2 for the locations of the cross sections.
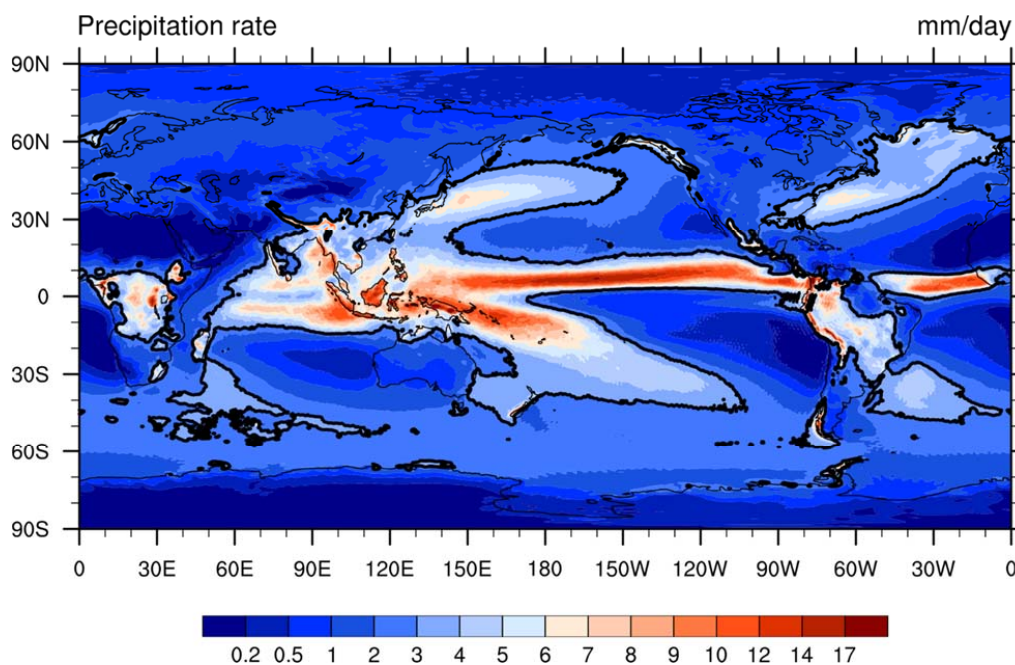
**Figure 13.** Annual mean precipitation rate (mm day$^{-1}$) from BCC-CSM2-HR. The 3 mm day$^{-1}$ contour is included in bold for reference.